RESEARCH ARTICLE

(CN4H7)2SO4·H2O: high-performance metal-free ultraviolet birefringent crystal with KBBF-like configuration†

Xia Hao,*[a] Sijing Xie,[a] Ruijie Wang,[a] Chensheng Lin, [ID][b] Lingli Wu,[b] Guang Peng, [ID][c] Tao Yan, [ID][b] Ning Ye [ID][c] and Min Luo [ID]*[b]

The advancement of high-quality ultraviolet (UV) birefringent crystalline materials is pivotal in advancing optoelectronic functional crystal technology. The outstanding birefringent fundamental group is indispensable for synthesizing target crystals that meet high-performance optical requirements. This study selected the $[CN_4H_7]^+$ group with a wide HOMO−LUMO gap and substantial polarizability anisotropy. Furthermore, by modifying the $KBe_2BO_3F_2$ (KBBF) template structure at the molecular level, the first metal-free sulfate $(CN_4H_7)_2SO_4 \cdot H_2O$ was successfully synthesized. This crystal effectively balanced the short UV cut-off edge (212 nm) and large birefringence (0.132@546.1 nm). Theoretical calculations indicated that $[CN_4H_7]^+$ group and its favorable arrangement were primarily responsible for the large birefringence. Our study reveals that coupling the $[CN_4H_7]^+$ group to tetrahedral frameworks serves as an effective approach to engineering UV birefringent crystals with enhanced optical anisotropy.

Introduction

The quantification of optical anisotropy in crystals is fundamentally governed by birefringence (Δn), a critical parameter enabling polarization control and angular phase-matching (PM).[1–8] High-performance birefringent materials have been demonstrated to be essential for controlling polarized light and realizing the functions of various linear optical devices, fiber optic sensors, and advanced optical communication systems.[9–14] Hitherto, despite serving as mainstream commercial UV birefringent crystals, MgF_2,[15] $CaCO_3$,[16] and α-BaB_2O_4 (α-BBO)[17] exhibit intrinsic limitations that constrain their widespread deployment. Hence, with the rapid development of both scientific and industrial communities, designing novel UV birefringent materials with superior performance is urgently needed.

Although non-π-conjugated $[SO_4]^{2-}$ with wide band gaps have garnered significant interest, their practical utilization remains constrained by limited birefringence.[18–22] Enhancing the birefringence typically involves strategic incorporation of birefringence-active units, including planar π-conjugated groups, stereochemically active lone-pair-containing metal cations,[23–25] d^0 cation octahedra with second-order Jahn–Teller distortions,[26–28] or d^{10} transition metal.[29,30] However, metal-based units often reduce band gap, compromising their UV/deep-UV applicability. The π-conjugated structural units, such as $[BO_3]$,[31] $[B_3O_6]$,[32] $[CO_3]$,[33] $[NO_3]$,[34] $[H_xC_3N_3O_3](x = 0, 1, 2,$ and $3)$,[35] $[C_3N_6H_7]$,[36] $[C(NH_2)_3]$[37] and $[CN_4H_7]$[38] have been extensively explored as critical design units for high-performance birefringent crystals. Notably, the $[CN_4H_7]$ group within π-conjugated systems has recently garnered significant attention owing to its exceptional optical characteristics: a wide HOMO–LUMO (the highest occupied molecular orbital-lowest unoccupied molecular orbital) gap (5.98 eV) and substantial polarizability anisotropy (21.68 a.u.),[38] attributed to strong covalent C–N bonds interactions and planar π-conjugated configurations, respectively. Furthermore, the coplanar hydrogen atoms in $[CN_4H_7]^+$ cation enable directional hydrogen bonding with electronegative N/O/F atoms, effectively restricting molecular module spatial freedom. This design strategy has yielded superior-performing compounds, including $[CN_4H_7]_2$ $[B_3O_3F_4(OH)]$ (195 nm, 0.161@1064 nm),[39] $(CN_4H_7)B_5O_6(OH)_4$ (198 nm, 0.126@532 nm),[40] $[CN_4H_7]H_2PO_2$ (214 nm, 0.144@532 nm),[41] $(CN_4H_7)HPO_2(OH)$ (196 nm, 0.144@532 nm),[41] $CN_4H_7SO_3CH_3$ (198 nm, 0.107@546 nm),[38] $CN_4H_7SO_3CF_3$ (183 nm, 0.149@546 nm)[38] and $(CN_4H_7)SO_3NH_2$ (6.11 eV, 0.155@546 nm).[42] To synergistically optimize both bandgap and birefringence in sulfate systems, we propose

[a]*School of Materials Science and Engineering, Henan Normal University, Xinxiang 453007, P. R. China. E-mail: hhhaoxia@163.com*
[b]*Key Laboratory of Optoelectronic Materials Chemistry and Physics, Fujian Institute of Research on the Structure of Matter, Chinese Academy of Sciences, Fuzhou, Fujian 350002, P. R. China. E-mail: lm8901@fjirsm.ac.cn*
[c]*Tianjin Key Laboratory of Functional Crystal Materials, Institute of Functional Crystal, Tianjin University of Technology, Tianjin 300191, China*

This journal is © the Partner Organisations 2025

Inorg. Chem. Front., 2025, **12**, 5335–5343 | 5335

incorporating planar π-conjugated $[CN_4H_7]^+$ functional units, which may achieve wide band gaps while amplifying optical anisotropy.

Furthermore, the parallel spatial layout of the functional units matters as well, given that it can benefit the optical anisotropy of crystals.[43,44] In $KBe_2BO_3F_2$, every $[BO_3]$ unit orderly links to $[BeO_3F]$ units, creating parallel-arranged $(Be_2BO_3F_2)_\infty$ layers that exhibit evident structural anisotropy. As a result, $KBe_2BO_3F_2$ has a substantial birefringence, leading to the short output wavelength for the second harmonic generation PM output wavelength (~161 nm).[45] In addition, a series of compounds with KBBF-like configurations also showed excellent optical properties, $NH_4Be_2BO_3F_2$ (173.9 nm, 0.0776@407 nm),[46] γ-Be_2BO_3F (146 nm, 0.1@532 nm),[46] $NH_4B_4O_6F$ (158 nm, 0.1171@1064 nm),[47] $Zn_2BO_3(OH)$ (204 nm, 0.067@800 nm),[48] $CN_4H_7SO_3CF_3$ (183 nm, 0.149@546 nm),[38] $C(NH_2)_3ClO_4$ (200 nm, 0.076@1064 nm),[49] $C(NH_2)_3SO_3F$ (~200 nm, 0.133@1064 nm),[37] $[C_2N_4H_7O][NH_2SO_3]$ (227 nm, 0.225@1064 nm).[50] Hence, manipulating the arrangement of functional modules is crucial in the design of birefringent materials.

We propose a strategic integration of planar π-conjugated $[CN_4H_7]^+$ group exhibiting a wide band gap and large polarizability anisotropy into $[SO_4]^{2-}$ to engineer metal-free sulfate. Our efforts to explore new compounds in the sulfate system led to the first metal-free sulfate, $(CN_4H_7)_2SO_4·H_2O$, with a configuration similar to that of KBBF. $(CN_4H_7)_2SO_4·H_2O$ exhibits the short UV cut-off edge (212 nm) and a large birefringence (0.126@1064 nm). This meticulously designed strategy may open the window for exploring UV birefringent materials.

Experimental section

Reagents

All experimental chemicals were of analytical grade from commercial sources and used without further purification. $NaHSO_4$ (≥98.5%) and $C_2H_8N_4O_3$ (98.5%) were purchased from Adamas.

Synthesis

Single crystals of $(CN_4H_7)_2SO_4·H_2O$ were grown by evaporating in an aqueous solution at 40 °C for two days or hydrothermally at 90 °C for 3 hours. In synthesizing the title compound, $NaHSO_4$ and $C_2H_8N_4O_3$ with a 1:1 molar ratio were mixed, and then H_2O (7 mL) was added. Transparent single crystals were obtained, washed with deionized water, and dried in air.

Millimetre-level $(CN_4H_7)_2SO_4·H_2O$ crystal was grown *via* the evaporated water solution. The reaction mixture of $NaHSO_4$ (3.30 g), $C_2H_8N_4O_3$ (3.74 g), and 70 mL H_2O was directly put into the 100 mL glass beaker. The oven was slowly heated to 40 °C and evaporated at this temperature for 7 days. Millimetre-level bulk crystals of $(CN_4H_7)_2SO_4·H_2O$ were obtained (Fig. S1†)

Single crystal X-ray diffraction

Single crystal X-ray diffraction data for $(CN_4H_7)_2SO_4·H_2O$ was collected by mounting these transparent crystals on glass fibers

with epoxy and using a SuperNova CCD diffractometer with graphite-monochromatic Cu Kα radiation (λ = 1.54184 Å) at 293 (2) K. Crystal structures of $(CN_4H_7)_2SO_4·H_2O$ was determined using direct methods. The obtained data was also solved and refined by difference Fourier maps and full-matrix least-squares fitting on F^2 using the SHELXS crystallographic software package for $(CN_4H_7)_2SO_4·H_2O$.[51] In addition, the structure was checked with the PLATON[52] program, and no higher symmetries were found. Details of the crystallographic data and structure refinement for $(CN_4H_7)_2SO_4·H_2O$ are presented in Table 1. Atomic coordinates, isotropic displacement coefficients, bond lengths, and bond angles are summarized in Tables S1–S3 of the ESI.†

Powder X-ray diffraction

The powder X-ray diffraction (XRD) patterns of $(CN_4H_7)_2SO_4·H_2O$ were collected using an Empyrean powder X-ray diffractometer with Cu Kα radiation (λ = 1.54059 Å) at room temperature. The pattern was recorded in the angular range of 2θ = 5–80° with a scan step width of 0.05°. The obtained XRD patterns of the pure powder samples showed excellent agreement with the calculated XRD patterns based on the single-crystal models (Fig. S2†).

Energy-dispersive X-ray spectroscopy analysis

Microprobe elemental analysis was conducted using a field emission scanning electron microscope (SUPRA® 40, Zeiss) with an energy-dispersive X-ray spectroscopy (EDS) detector. The results confirmed the presence of C, N, S, and O elements, which correspond well with the chemical formula of $(CN_4H_7)_2SO_4·H_2O$. The EDS spectrum for the title compound is shown in the ESI (Fig. S3†).

Thermal analysis

The thermal properties of $(CN_4H_7)_2SO_4·H_2O$ were measured on a NETZSCH STA449F5A simultaneous analyzer with an Al_2O_3

Table 1 Crystal data and structure refinement of $(CN_4H_7)_2SO_4·H_2O^a$

Formula	$C_2H_{16}N_8O_5S$
Formula weight (g mol^{-1})	264.29
Crystal system	Orthorhombic
Space group	*Pnma*
Temperature/K	293(2)
a (Å)	6.7623(2)
b (Å)	14.1499(4)
c (Å)	11.6621(3)
α/°	90.00
β/°	90.00
γ/°	90.00
V/Å^3	1115.90(5)
Z	4
ρ(calc.) g cm^{-3}	1.573
μ/mm^{-1}	2.891
$F(000)$	560.0
λ (Å)	1.54184
GOF on F^2	1.092
R/wR ($I \geq 2\sigma(I)$)	R_1 = 0.0479, wR_2 = 0.1143
R/wR (all data)	R_1 = 0.0496, wR_2 = 0.1165

^{a} $R(F) = \sum ||F_o| - |F_c||/\sum|F_o|$·w$R(F_o^2) = [\sum w(F_o^2 - F_c^2)^2/\sum w(F_o^2)^2]^{\frac{1}{2}}$.

crucible as the reference. Heated the powder samples weighing 16.185 mg in an Al_2O_3 crucible from 23 to 800 °C at a rate of 10 K min^{-1} under a constant flow of nitrogen (Fig. S6†).

UV–Vis–NIR diffuse reflectance spectroscopy

At room temperature, the UV-vis-NIR diffuse reflectance spectra of $(CN_4H_7)_2SO_4 \cdot H_2O$ were measured with a PerkinElmer Lambda-1050 UV/vis/NIR spectrophotometer. Moreover, the tested wavelength range of $(CN_4H_7)_2SO_4 \cdot H_2O$ was 200–1500 nm, with pure BaSO4 powder as the reference sample of 100% reflectance (Fig. 2).

IR absorption spectra

The infrared absorption spectra of $(CN_4H_7)_2SO_4 \cdot H_2O$ in the wavenumber range of 400–4000 cm^{-1} were recorded using an ALPHA II model wireless Fourier-transform infrared (FT-IR) spectrometer (conventional mode). The 2–3 mg of dried sample powder was placed in the sample area of the instrument, compressed into a pellet, and the instrument position was properly adjusted prior to measurement.

Birefringence

The birefringences of $(CN_4H_7)_2SO_4 \cdot H_2O$ were obtained through the polarizing microscope (ZEISS Axio Scope. A1) equipped with 546.1 nm light. In the experiment, clean and transparent lamellar crystals were chosen to improve the accuracy of the test. The following formula was listed to calculate birefringence:

$$R = (|Ne-No|) \times T = \Delta n \times T \qquad (1)$$

R denotes optical path difference, Δn represents birefringence, and T means the crystal's thickness.

The first-principles calculation

The electronic structures of the single-crystal $(CN_4H_7)_2SO_4 \cdot H_2O$ without further optimization were calculated by the density functional theory (DFT) method with CASTEP[53] code in the Material Studio package. The exchange and correlative potential of electron–electron interactions were treated by the generalized gradient approximation (GGA) with the scheme of Perdew–Burke–Ernzerhof (PBE)[54] form. The norm-conserving pseudo potential was used to show the interactions between the ionic core and valence electrons. Moreover, the following orbital electrons were regarded as the valence electrons: H, 1s1; C, 2s2 2p2; N, 2s2 2p3; O, 2s2 2p4; S, 3s2 3p4. The cut-off energy of $(CN_4H_7)_2SO_4 \cdot H_2O$ was 750 eV. The convergence criteria of total energy for $(CN_4H_7)_2SO_4 \cdot H_2O$ was set to 1.0×10^{-5} eV per atom, and the k-points sampling of $2 \times 1 \times 1$ in the first Brillouin zone were respectively selected for calculation according to the Monkhorst–Pack[55] scheme.

Results and discussion

Crystal structure

$(CN_4H_7)_2SO_4 \cdot H_2O$ crystallizes in the orthorhombic crystal system with a symmetric space group of *Pnma* (62) (Table 1).

The unit cell parameters are a = 6.7623(2) Å, b = 14.1499(4) Å, c = 11.6621(3) Å, α = 90.00°, β = 90.00°, γ = 90.00° and z = 4. The basic structural units of $(CN_4H_7)_2SO_4 \cdot H_2O$ contained one set of crystallographically unique C, N, H, S, and O atoms. Each C and N atoms are connected by three types of bonds, C–N, N–N, and N–H, forming a planar π-conjugated $[CN_4H_7]^+$ cation. The compound has typical bond distances: C–N is 1.315–1.330 Å, N–N is 1.408 Å, and N–H is 0.861–0.872 Å (Fig. S4†). In addition, the N–C–N angles range from 118.198° to 121.178°, and the C–N–N angles range between 119.414° (Fig. S4†). The tetrahedral anionic group, $[SO_4]^{2-}$, has a typical bond distance of S–O of 1.467–1.474 Å, and the O–S–O angles range from 107.873° to 110.025° (Fig. S4†). As shown in Fig. 1b, the isolated π-conjugated $[CN_4H_7]^+$ groups interact with H_2O molecules, $[SO_4]^{2-}$ tetrahedrons, and $[CN_4H_7]^+$ groups, respectively. Moreover, these interactions are linked *via* N–H···O$_{water}$, N–H···O$_{(SO4)}$, O–H···O$_{(SO4)}$ and N–H···N hydrogen bonds, forming a two-dimensional (2D) $[(CN_4H_7)_2SO_4 \cdot H_2O]_\infty$ layer. The 2D $[(CN_4H_7)_2SO_4 \cdot H_2O]_\infty$ layers are oriented at a fixed angle of 21.99° with respect to the crystallographic b-axis (Fig. 1d). The structure of $(CN_4H_7)_2SO_4 \cdot H_2O$ is made of electroneutral $[(CN_4H_7)_2SO_4 \cdot H_2O]_\infty$ layers stacking along the a-axis by hydrogen bond (Fig. S5†). Notably, the O atoms of H_2O molecules and the S atoms within $[SO_4]^{2-}$ are arranged in the ac plane, forming a coherent stacking arrangement along the b-axis. This unique configuration enables $[CN_4H_7]^+$ groups with significant optical anisotropy to adopt uniform parallel alignment within the lattice along the a-axis (Fig. 1d).

The structure of $(CN_4H_7)_2SO_4 \cdot H_2O$ is remarkably similar to that of the well-known KBBF, as initially envisaged. As shown in Fig. S1a–1d,† $(CN_4H_7)_2SO_4 \cdot H_2O$ inherits the structural advantages of KBBF and achieves an almost coplanar arrangement of $[CN_4H_7]^+$ groups, which enhances the birefringence of sulfate. But $[CN_4H_7]^+$ and $[SO_4]^{2-}$ groups in this crystal are arranged antiparallel, causing their dipole moments to completely cancel each other out, which is conducive to the centrosymmetric structure. The 2D $[(CN_4H_7)_2SO_4 \cdot H_2O]_\infty$ layer is similar to the $[Be_2BO_3F]_\infty$ layer in KBBF. Compared to KBBF, the layer spacing of $(CN_4H_7)_2SO_4 \cdot H_2O$ significantly reduced from 6.25 to 3.38 Å, leading to an increase in the density of the functional units, which is beneficial for the further enhancement of the $(CN_4H_7)_2SO_4 \cdot H_2O$ birefringence.

Thermal analysis

As shown in Fig. S6,† the TG and DSC curves of $(CN_4H_7)_2SO_4 \cdot H_2O$ show that it remains stable up to 82 °C. Besides, it exhibits two main steps of weight loss in 23–800 °C, corresponding to the release of 1 mol H_2O with a weight loss of 6.80% (cal. 6.81%) in the first stage, and 1 mol $(CN_4H_7)_2SO_4$ with a weight loss of 91.45% (cal. 93.19%) for the second stage. In practical applications, surface coating and physical encapsulation techniques can improve the high-temperature stability of $(CN_4H_7)_2SO_4 \cdot H_2O$.

UV-Vis-NIR diffuse reflectance spectroscopy

The UV-vis-NIR diffuse reflectance spectra were measured and are shown in Fig. 2. It is clear that the UV cut-off edge of
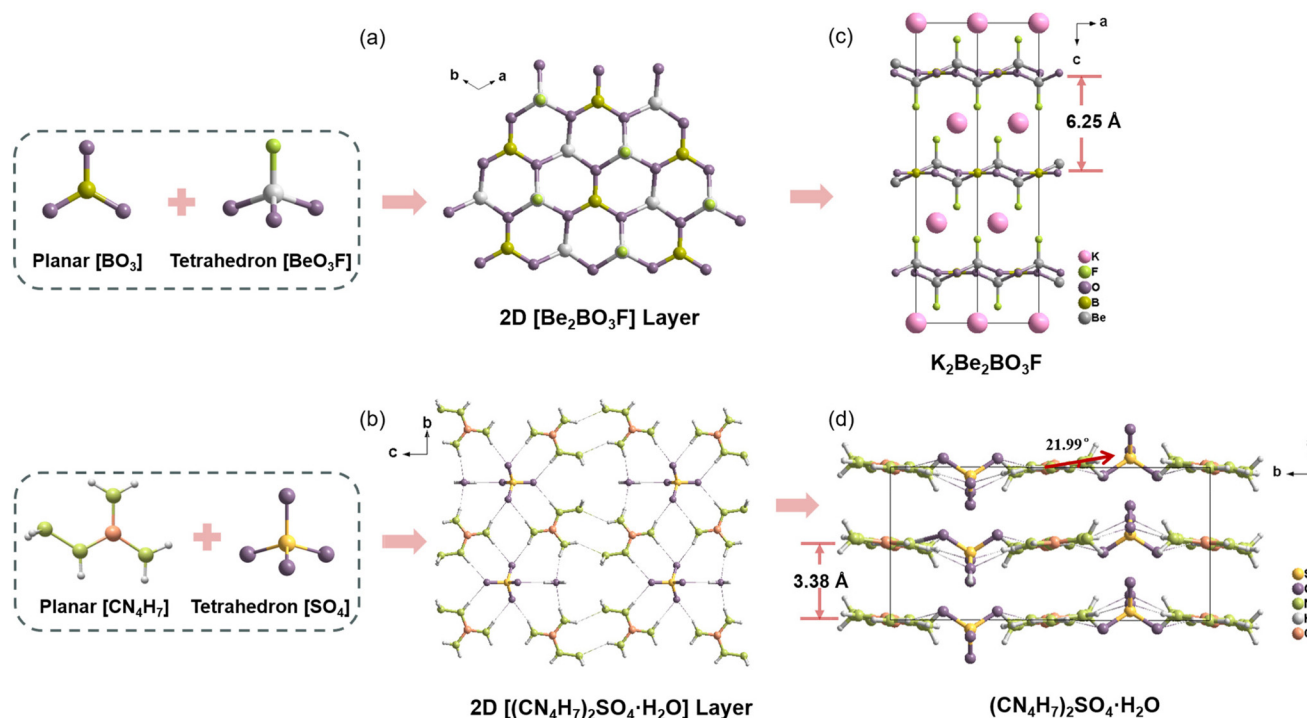
This journal is © the Partner Organisations 2025

Inorg. Chem. Front., 2025, **12**, 5335–5343 | **5337**

Fig. 1 The structure of $(CN_4H_7)_2SO_4 \cdot H_2O$ and the structural comparison between $(CN_4H_7)_2SO_4 \cdot H_2O$ and KBBF: (a) the 2D $[Be_2BO_3F_2]_\infty$ layers in KBBF structure; (b) the planar $[CN_4H_7]^+$ groups connect with $[SO_4]$ tetrahedron and $[H_2O]$ molecule *via* the N–H⋯O hydrogen bonds to form the 2D $[(CN_4H_7)_2SO_4 \cdot H_2O]_\infty$ layers; (c) the $[Be_2BO_3F_2]_\infty$ layers stack along *c* axis in the KBBF; (d) the $[(CN_4H_7)_2SO_4 \cdot H_2O]_\infty$ layers stack along *a*-axis in $(CN_4H_7)_2SO_4 \cdot H_2O$.
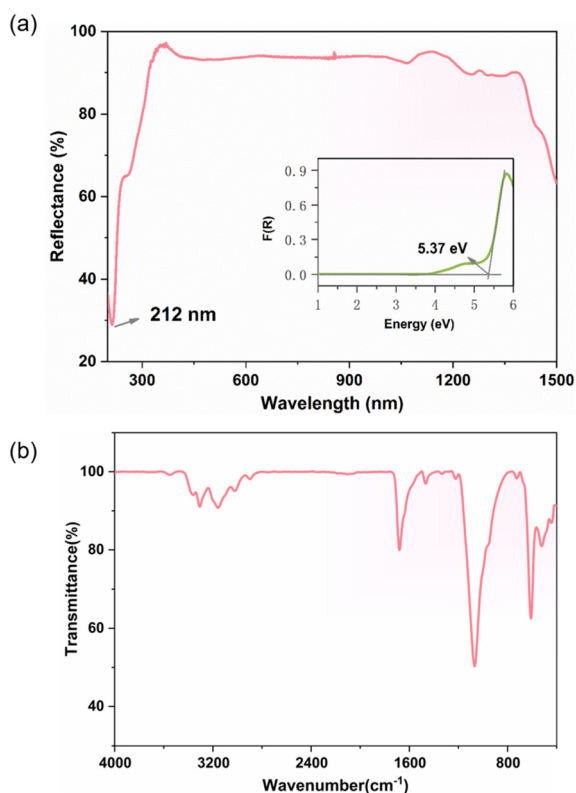
Fig. 2 (a) The UV-Vis-NIR diffuse reflectance spectra; (b) IR spectrum of $(CN_4H_7)_2SO_4 \cdot H_2O$.

$(CN_4H_7)_2SO_4 \cdot H_2O$ powder samples is 212 nm. The absorptance curve of $(CN_4H_7)_2SO_4 \cdot H_2O$ transformed using the Kubelka–Munk function,[56,57] $F(R) = (1 - R)^2/2R = K/S$ (R is the reflectance, K is the absorption, and S is the scattering), led to an estimated band gap of 5.37 eV. It is worth noting that this UV cut-off edge is shorter than most of the reported ionic organic materials, such as $(NH_4)_2Zn(SCN)_4 \cdot 3H_2O$ (297 nm),[58] $[C(NH_2)_3]_2SO_3S$ (254 nm),[59] $Zn(SCN)_2$ (259 nm),[58] $Ba(H_2C_6N_7O_3)_2 \cdot 8H_2O$ (302 nm),[60] $Cd(H_2C_6N_7O_3)_2 \cdot 8H_2O$ (310 nm)[61] and $C(NH_2)_3IO_3$ (242 nm).[62] It is also greater than that of many reported sulfate crystals (Table S4† and Fig. 4). The above test results demonstrate that $(CN_4H_7)_2SO_4 \cdot H_2O$ can meet the requirements for applications in the short-wave UV region.

IR absorption spectra

According to the infrared spectrum shown in Fig. 2b, the absorption peaks at 3548 and 723 cm^{-1} correspond to the O–H stretching vibrations and bending vibrations of water molecules, respectively. The bands at 3308 and 3360 cm^{-1} are attributed to the symmetric and asymmetric stretching vibrations of N–H bonds, while the peak at 1680 cm^{-1} arises from the scissoring vibrations of N–H groups. The 1468 cm^{-1} feature reflects coupled vibrations involving C–N single-bond stretching and N–H bending modes, and the 1332 cm^{-1} band is assigned to the asymmetric stretching vibration of C–N bonds under hydrogen-bonding perturbation. The presence of

5338 | *Inorg. Chem. Front.*, 2025, **12**, 5335–5343

This journal is © the Partner Organisations 2025

N–N bonds, confirmed by single-crystal structural analysis, validates the existence of the $(CN_4H_7)^+$ cation. Additionally, the symmetric and asymmetric stretching vibrations of S–O bonds are observed at 1069 and 1223 cm^{-1}, respectively, with their bending vibrations appearing at 609, 521, and 440 cm^{-1}, collectively confirming the $(SO_4)^{2-}$ anion in the structure.

Electronic structure calculation

To gain further insight into the mechanism behind the optical properties, the first-principles method was applied to the electronic and optical properties of $(CN_4H_7)_2SO_4 \cdot H_2O$. Band struc-

ture calculations revealed that the direct band gap of the titled compound is 4.33 eV (Fig. S7†), which is smaller than the experimental value (5.37 eV) because the eigenvalues of the electronic states did not accurately describe the DFT-GGA, resulting in the quantitative underestimation of optical band gaps. Hence, the scissor value of 1.04 eV was used to move up the conduction bands to keep with the experimental value for an accurate calculation of optical properties. It is known that electron transitions in the upper region of the valence band and the bottom of the conduction band primarily determine optical properties. Based on the partial densities of states near
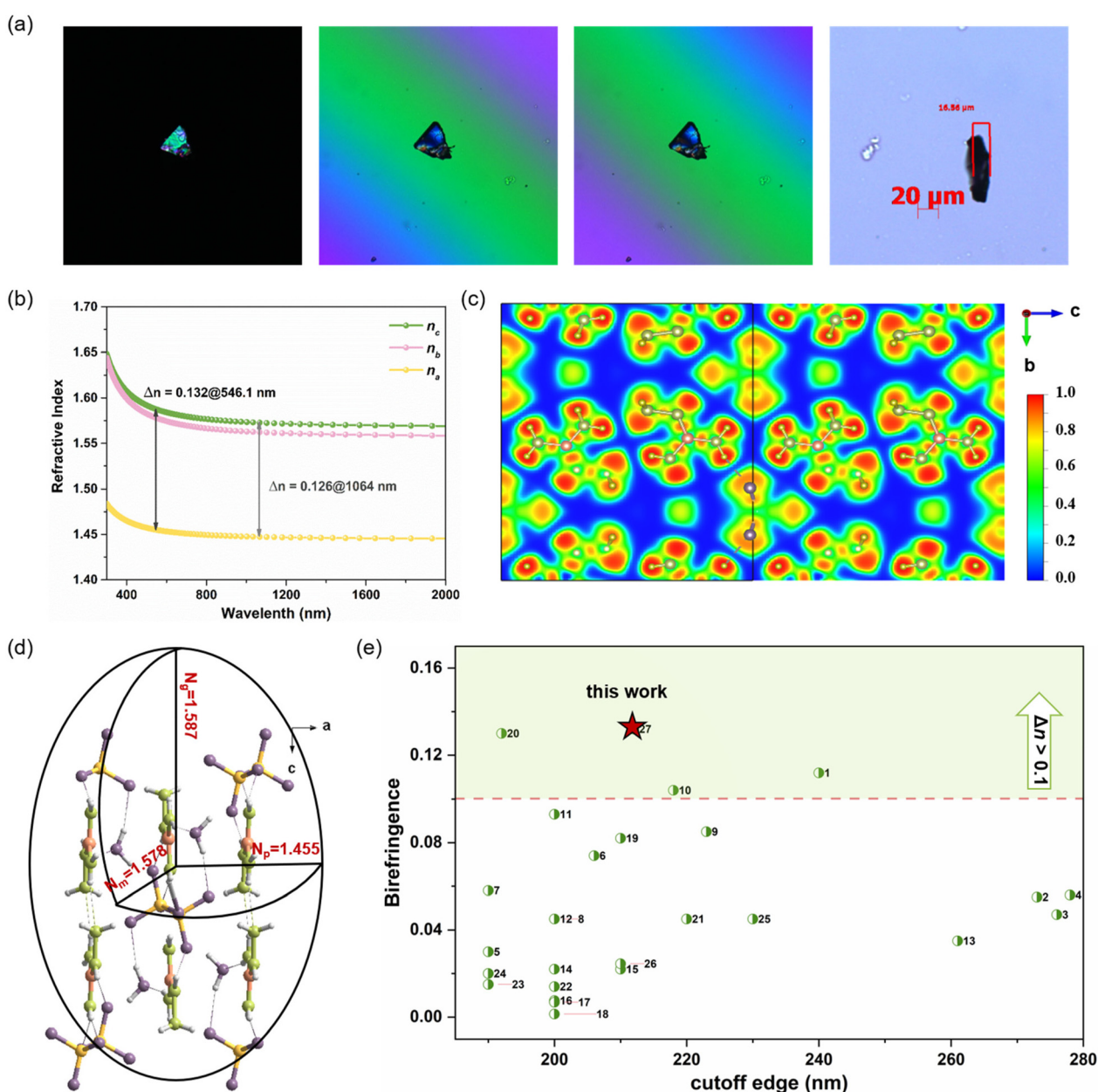

Fig. 3 The analysis of birefringence in crystal $(CN_4H_7)_2SO_4 \cdot H_2O$: (a) the photograph of the measured birefringence; (b) the refractive index; (c) the ELF diagram of $[CN_4H_7]^+$, H_2O and $[SO_4]^{2-}$ in *bc* plane; (d) the diagrammatic sketch of functional modules in an optical indicatrix (Ng > Nm > Np) at 546.1 nm; (e) the cut-off edges and birefringence of UV sulfates (<280 nm), the number corresponds to the compounds listed in Table S4.†

This journal is © the Partner Organisations 2025

Inorg. Chem. Front., 2025, **12**, 5335–5343 | **5339**

the Fermi level, which were primarily composed of H 1s, C 2p, N 2p, and O 2p orbitals, with a small contribution from the S 3p state (PDOS, Fig. 4). It can be concluded that the band gap of $(CN_4H_7)_2SO_4·H_2O$ is determined by the π-conjugated unit $[CN_4H_7]^+$ and tetrahedra $[SO_4]^{2-}$ groups.

Mechanism of birefringence

The birefringences of $(CN_4H_7)_2SO_4·H_2O$ were tested on a ZEISS Axio Scope A1 equipped with a Berek compensator. The measurement results exhibited that the retardation values of the measured crystal were approximately 1929.95 nm, respectively, and the thicknesses of them were 16.56 μm, respectively (Fig. 3a). According to eqn (1), the calculated birefringences were 0.117@546.1 nm (Table 2). In addition, a systematic investigation into the refractive indices was initiated, employing first-principles calculations to analyze its optical characteristics. $(CN_4H_7)_2SO_4·H_2O$ crystallizes in the orthorhombic crystal system, and thus it is a biaxial crystal. The calculated refractive indices of $(CN_4H_7)_2SO_4·H_2O$ are n_c = 1.573/1.587, n_b = 1.562/1.578, and n_a = 1.447/1.455 at 1064/546.1 nm, respectively (Fig. 3b). Therefore, it showed strong optical anisotropy with large birefringences of 0.126@1064 nm and 0.132@546.1 nm, which is in good agreement with the experimental value (0.117@546.1 nm). It is worth noting that the birefringence of $(CN_4H_7)_2SO_4·H_2O$ is larger than the practical crystals, including MgF_2 (0.013@253.7 nm),[15] LiB_3O_5 (LBO) (0.04@1064 nm)[63] and $CsLiB_6O_{10}$ (CLBO) (0.049@1064 nm).[64] Besides, its birefringence exceeds many reported UV sulfate crystals (<280 nm). In these reported short-wave UV sulfate crystals, only three compounds exhibit a birefringence greater than 0.1: $CsSbF_2SO_4$ (0.112@1064 nm), $NH_3SO_3(NH_4)_2SO_4$ (0.104@520 nm) and $NaLa(SO_4)_2(H_2O)$ (0.13@1064 nm). Additionally, $(CN_4H_7)_2SO_4·H_2O$ demonstrates the largest birefringence among all sulfate compounds in the UV region below 280 nm (Fig. 4e and Table S4†). $(CN_4H_7)_2SO_4·H_2O$ exhibits a high birefringence (0.117@546.1 nm$^{exp.}$ and 0.132@546.1 nm$^{cal.}$), with its experimental value being 9-fold greater than that of MgF_2 (0.013@253.7 nm) and comparable to α-BBO (0.12@532 nm).[17] This property enables optimized polarization-state control efficiency, facilitates compact optical device design, reduces system volume, and lowers complexity, providing a foundation for device miniaturization. Furthermore, the enhanced phase retardation achieved by high-birefringence materials in the UV spectrum directly addresses the performance requirements of precision optical systems.

Why does $(CN_4H_7)_2SO_4·H_2O$ exhibit such a large birefringence? Firstly, theoretical calculations indicate that the $[CN_4H_7]^+$ group exhibits high anisotropic polarizability (21.68 a.u.).
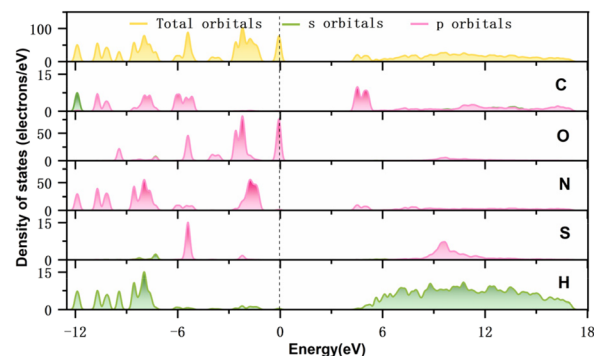

Fig. 4 The total and partial density of states.

Additionally, the electron localization function (ELF, Fig. 3c) diagram intuitively reveals that the $[CN_4H_7]^+$ group possesses the typical π-conjugated electronic configuration and the asymmetrical electronic distributions around $[CN_4H_7]^+$. Secondly, the arrangement of $[CN_4H_7]^+$, H_2O and $[SO_4]^{2-}$ units in 2D $[(CN_4H_7)_2SO_4·H_2O]_\infty$ layer is constrained by intralayer N–H···O$_{water}$, N–H···O$_{(SO4)}$, O–H···O$_{(SO4)}$ and N–H···N hydrogen bonding interactions. Meanwhile, the two π-conjugated $[CN_4H_7]^+$ units in adjacent 2D layers are parallel (Fig. 1d and 3d). From the a-axis perspective, the nearly perfect overlap of C atoms in adjacent $[CN_4H_7]^+$ units creates significant repulsion between neighboring $[CN_4H_7]^+$ units (Fig. S8†). Moreover, due to the repulsion between the lone pair electrons on N1 in the group $[CN_4H_7]^+$, the adjacent $[CN_4H_7]^+$ groups along the a-axis direction undergo rotation (Fig. S8†). The $[CN_4H_7]^+$ unit is modulated by the synergies between hydrogen bonds and repulsive forces, thereby increasing the optical anisotropy of $(CN_4H_7)_2SO_4·H_2O$. Lastly, the interlayer distance of the title compound is smaller than that of KBBF, which is conducive to accommodating more $[CN_4H_7]^+$ groups, thereby enhancing the birefringence.

In addition, we put π-conjugated $[CN_4H_7]^+$ units, H_2O molecule, and tetrahedra $[SO_4]$ in an optical indicatrix to demonstrate the optical anisotropy of $(CN_4H_7)_2SO_4·H_2O$ more intuitively. In Fig. 3d, the direction of the maximum refractive index (N_g) is the c-axis, which results from a small angle of 7.7° between the c-axis and the $[CN_4H_7]^+$ unit. The medium refractive index (N_m) lies along the b-axis, primarily due to the 21.99° angle between group $[CN_4H_7]^+$ and the b-axis, significantly larger than the 7.7° angle mentioned earlier. This angular stems from the presence of H_2O molecules in the 2D $[(CN_4H_7)_2SO_4·H_2O]_\infty$ layer, where hydrogen bond N–H···O$_{water}$ from $[CN_4H_7]^+$ units and O–H···O$_{(SO4)}$ hydrogen bond from $[SO_4]^{2-}$ units. Concurrently, the opposite alignment of H_2O molecules within the 2D layer forces the $[CN_4H_7]^+$ and $[SO_4]^{2-}$ units to deviate from coplanar alignment. The direction of the minimum refractive index (N_p) is along the a-axis because the a-axis is almost perpendicular to the plane $[CN_4H_7]^+$.

Conclusions

In this study, to discover short-wave UV birefringent crystals with large birefringence in sulfate systems, we combined high-

Table 2 The calculated and experimental values of the birefringence (Δn) for $(CN_4H_7)_2SO_4·H_2O$

Crystal	Calculated Δn (λ = 546.1 nm)	Experimental
$(CN_4H_7)_2SO_4·H_2O$	0.132	0.117

performance birefringent functional group $[CN_4H_7]^+$ with sulfate groups. Based on the KBBF template structure, the first metal-free $(CN_4H_7)_2SO_4 \cdot H_2O$ was successfully designed and synthesized to achieve an effective balance between a short UV cut-off edge (212 nm) and large birefringence (0.132@546.1 nm). Moreover, the combined influence of the $[CN_4H_7]^+$ and $(SO_4)^{2-}$ groups contributes to the optical properties of $(CN_4H_7)_2SO_4 \cdot H_2O$. Our research provides a novel and effective approach to enhancing tetrahedron-based birefringence while maintaining a short UV cut-off edge, offering insights into exploring novel UV birefringent materials.

Author contributions

Xia Hao: conceptualization, methodology, validation, formal analysis, resources, writing-original draft, writing – review & editing, visualization, supervision, project administration, and funding acquisition; Sijing Xie, Lingli Wu: investigation; Ruijie Wang: visualization; Chensheng Lin: formal analysis; Guang Peng, Tao Yan, Ning Ye: resources; Min Luo: supervision, resources. All authors contributed to the general discussion. All authors agree with the final version of the manuscript.

Data availability

The authors confirm that the data supporting the findings of this study are available within the article [and/or its ESI†].

Conflicts of interest

There are no conflicts to declare.

Acknowledgements

References

1 Z. S. Lin, Z. Z. Wang, C. T. Chen and M. H. Lee, Mechanism of linear and nonlinear optical effects of KDP and urea crystals, *J. Chem. Phys.*, 2003, **118**, 2349–2356.

2 W. J. Yao, R. He, X. Y. Wang, Z. S. Lin and C. T. Chen, Analysis of Deep-UV Nonlinear Optical Borates: Approaching the End, *Adv. Opt. Mater.*, 2014, **2**, 411–417.

3 B. B. Zhang, G. Q. Shi, Z. H. Yang, F. F. Zhang and S. L. Pan, Fluorooxoborates: Beryllium-Free Deep-Ultraviolet Nonlinear Optical Materials without Layered Growth, *Angew. Chem., Int. Ed.*, 2017, **56**, 3916–3919.

4 M. Mutailipu, M. Zhang, B. B. Zhang, L. Y. Wang, Z. H. Yang, X. Zhou and S. L. Pan, $SrB_5O_7F_3$ Functionalized with $[B_5O_9F_3]^{6-}$ Chromophores: Accelerating the Rational Design of Deep-Ultraviolet Nonlinear Optical Materials, *Angew. Chem., Int. Ed.*, 2018, **57**, 6095–6099.

5 M. F. Wu, E. Tikhonov, A. Tudi, I. Kruglov, X. L. Hou, C. W. Xie, S. L. Pan and Z. H. Yang, Target-Driven Design of Deep-Ultraviolet Nonlinear Optical Materials Based on Explainable Machine Learning, *Adv. Mater.*, 2023, **35**, 2300848.

6 M. Yan, C. L. Hu, R. L. Tang, W. D. Yao, W. L. Liu and S. P. Guo, $KBa_3M_2F_{14}Cl$ (M = Zr, Hf): novel short-wavelength mixed metal halides with the largest second-harmonic generation responses contributed by mixed functional moieties, *Chem. Sci.*, 2024, **22**, 8253–8859.

7 X. F. Wang, X. D. Leng, Y. S. Kuk, J. Lee, Q. Jing and K. M. Ok, Deep-Ultraviolet Transparent Mixed Metal Sulfamates with Enhanced Nonlinear Optical Properties and Birefringence, *Angew. Chem., Int. Ed.*, 2023, **63**, e202315434.

8 Z. Y. Bai and K. M. Ok, Designing Sulfate Crystals with Strong Optical Anisotropy through π-Conjugated Tailoring, *Angew. Chem., Int. Ed.*, 2024, **63**, e202315311.

9 M. F. Weber, C. A. Stover, L. R. Gilbert, T. J. Nevitt and A. J. Ouderkirk, Giant Birefringent Optics in Multilayer Polymer Mirrors, *Science*, 2000, **287**, 2451–2456.

10 Z. Y. Xie, L. G. Sun, G. Z. Han and Z. Z. Gu, Optical Switching of a Birefringent Photonic Crystal, *Adv. Mater.*, 2008, **20**, 3601–3604.

11 M. Mutailipu, K. R. Poeppelmeier and S. L. Pan, Borates: A Rich Source for Optical Materials, *Chem. Rev.*, 2021, **121**, 1130–1202.

12 Y. Li and K. M. Ok, Breaking Boundaries: Giant Ultraviolet Birefringence in Dimension-Reduced Zn-Based Crystals, *Angew. Chem., Int. Ed.*, 2024, e202409336.

13 Z. H. Yang, A. Tudi, B. H. Lei and S. L. Pan, Enhanced nonlinear optical functionality in birefringence and refractive index dispersion of the deep-ultraviolet fluorooxoborates, *Sci. China Mater.*, 2020, **63**, 1480–1488.

14 M. Mutailipu, J. Han, Z. Li, F. M. Li, J. J. Li, F. F. Zhang, X. F. Long, Z. H. Yang and S. L. Pan, Achieving the full-wavelength phase-matching for efficient nonlinear optical frequency conversion in $C(NH_2)_3BF_4$, *Nat. Photonics*, 2023, **17**, 694–701.

15 F. Sedlmeir, R. Zeltner, G. Leuchs and H. G. L. Schwefel, High-Q MgF_2 whispering gallery mode resonators for refractometric sensing in aqueous environment, *Opt. Express*, 2014, **22**, 30934–30942.

16 G. Ghosh, Dispersion-equation coefficients for the refractive index and birefringence of calcite and quartz crystals, *Opt. Commun.*, 1999, **163**, 95–102.

17 G. Q. Zhou, J. Xu, X. D. Chen, H. Y. Zhong, S. T. Wang, K. Xu, P. Z. Deng and F. X. Gan, Growth and spectrum of a novel birefringent α-BaB_2O_4 crystal, *J. Cryst. Growth*, 1998, **191**, 517–519.

18 P. Hlubina, D. Ciprian and L. Knyblová, Interference of white light in tandem configuration of birefringent crystal

This journal is © the Partner Organisations 2025

Inorg. Chem. Front., 2025, **12**, 5335–5343 | **5341**

and sensing birefringent fiber, *Opt. Commun.*, 2006, **260**, 535–541.

19 C. Wu, T. H. Wu, X. X. Jiang, Z. J. Wang, H. Y. Sha, L. Lin, Z. S. Lin, Z. P. Huang, X. F. Long, M. G. Humphrey and C. Zhang, Large Second-Harmonic Response and Giant Birefringence of $CeF_2(SO_4)$ Induced by Highly Polarizable Polyhedra, *J. Am. Chem. Soc.*, 2021, **143**, 4138–4142.

20 Y. G. Lu, X. X. Jiang, C. Wu, L. Lin, Z. P. Huang, Z. S. Lin, M. G. Humphrey and C. Zhang, Molecular Engineering toward an Enlarged Optical Band Gap in a Bismuth Sulfate via Homovalent Cation Substitution, *Inorg. Chem.*, 2021, **60**, 5851–5859.

21 Y. Q. Zhao, Y. P. Song, Y. Q. Li, W. Liu, Y. Zhou, W. Q. Huang, J. H. Luo, S. G. Zhao and B. Ahmed, Deep-Ultraviolet Bialkali–Rare Earth Metal Anhydrous Sulfate Birefringent Crystal, *Inorg. Chem.*, 2024, **63**, 11187–11193.

22 C. Wu, X. X. Jiang, Y. L. Hu, C. B. Jiang, T. H. Wu, Z. S. Lin, Z. P. Huang, M. G. Humphrey and C. Zhang, A Lanthanum Ammonium Sulfate Double Salt with a Strong SHG Response and Wide Deep-UV Transparency, *Angew. Chem., Int. Ed.*, 2022, **61**, e202115855.

23 S. J. Han, A. Tudi, W. B. Zhang, X. L. Hou, Z. H. Yang and S. L. Pan, Recent Development of SnII, SbIII-based Birefringent Material: Crystal Chemistry and Investigation of Birefringence, *Angew. Chem., Int. Ed.*, 2023, **62**, e202302025.

24 Y. C. Liu, X. M. Liu, S. Liu, Q. R. Ding, Y. Q. Li, L. N. Li, S. G. Zhao, Z. S. Lin, J. H. Luo and M. C. Hong, An Unprecedented Antimony(III) Borate with Strong Linear and Nonlinear Optical Responses, *Angew. Chem., Int. Ed.*, 2020, **59**, 7793–7796.

25 P. F. Li, C. L. Hu, Y. F. Li, J. G. Mao and F. Kong, $Hg_4(Te_2O_5)(SO_4)$: A Giant Birefringent Sulfate Crystal Triggered by a Highly Selective Cation, *J. Am. Chem. Soc.*, 2024, **146**, 7868–7874.

26 T. H. Wu, X. X. Jiang, K. Duanmu, C. Wu, Z. S. Lin, Z. P. Huang, M. G. Humphrey and C. Zhang, Giant Optical Anisotropy in a Covalent Molybdenum Tellurite via Oxyanion Polymerization, *Adv. Sci.*, 2024, **11**, 2306670.

27 J. H. Wu, C. L. Hu, T. K. Jiang, J. G. Mao and F. Kong, Highly Birefringent d0 Transition Metal Fluoroantimonite in the Mid Infrared Band: Order–Disorder Regulation by Cationic Size, *J. Am. Chem. Soc.*, 2023, **145**, 24416–24424.

28 S. Liu, X. M. Liu, S. G. Zhao, Y. C. Liu, L. N. Li, Q. R. Ding, Y. Q. Li, Z. S. Lin, J. H. Luo and M. C. Hong, An Exceptional Peroxide Birefringent Material Resulting from d–π Interactions, *Angew. Chem., Int. Ed.*, 2020, **59**, 9414–9417.

29 C. X. Li, X. H. Meng, Z. Li and J. Y. Yao, Hg-based chalcogenides: An intriguing class of infrared nonlinear optical materials, *Coord. Chem. Rev.*, 2022, **453**, 214328.

30 Y. Chu, H. S. Wang, Q. Chen, X. Su, Z. X. Chen, Z. H. Yang, J. J. Li and S. L. Pan, "Three-in-One": A New Hg-Based Selenide Hg7P2Se12 Exhibiting Wide Infrared Transparency Range and Strong Nonlinear Optical Effect, *Adv. Funct. Mater.*, 2024, **34**, 2314933.

31 M. Zhang, D. H. An, C. Hu, X. L. Chen, Z. H. Yang and S. L. Pan, Rational Design via Synergistic Combination Leads to an Outstanding Deep-Ultraviolet Birefringent Li2Na2B2O5 Material with an Unvalued B2O5 Functional Gene, *J. Am. Chem. Soc.*, 2019, **141**(7), 3258–3264.

32 H. P. Wu, Z. J. Wei, Z. G. Hu, J. Y. Wang, Y. C. Wu and H. W. Yu, Assembly of π-Conjugated $[B_3O_6]$ Units by Mer-Isomer $[YO_3F_3]$ Octahedra to Design a UV Nonlinear Optical Material, $Cs_2YB_3O_6F_2$, *Angew. Chem., Int. Ed.*, 2024, e202406318.

33 G. Peng, C. S. Lin and N. Ye, $NaZnCO_3(OH)$: A High-Performance Carbonate Ultraviolet Nonlinear Optical Crystal Derived from $KBe_2BO_3F_2$, *J. Am. Chem. Soc.*, 2020, **142**, 20542–20546.

34 Q. Xia, X. Jiang, C. Jiang, H. Zhang, Y. Hu, L. Qi, C. Wu, G. Wei, Z. Lin, Z. Huang, M. G. Humphrey and C. Zhang, pH-Dependent Switching Between Nonlinear-Optical-Active Nitrate-Based Supramolecular Polymorphs, *Angew. Chem., Int. Ed.*, 2025, e202503136.

35 D. H. Lin, M. Luo, C. S. Lin, F. Xu and N. Ye, KLi $(HC_3N_3O_3) \cdot 2H_2O$: Solvent-drop Grinding Method toward the Hydro-isocyanurate Nonlinear Optical Crystal, *J. Am. Chem. Soc.*, 2019, **141**, 3390–3394.

36 H. Jia, D. Xu, Z. Li, M. Arif, Y. Jianga and X. Hou, $(C_3N_6H_7)$ $BF_4 \cdot H_2O$ and $(C_3N_6H_7)SO_3CH_3 \cdot H_2O$ with large birefringence induced by coplanar π-conjugated $[C_3N_6H_7]^+$ groups, *Inorg. Chem. Front.*, 2024, **11**, 8331–8338.

37 M. Luo, C. S. Lin, D. H. Lin and N. Ye, Rational Design of the Metal–Free $KBe_2BO_3F_2$ (KBBF) Family Member $C(NH_2)_3SO_3F$ with Ultraviolet Optical Nonlinearity, *Angew. Chem., Int. Ed.*, 2020, **59**, 16112–16115.

38 H. Zhou, M. Cheng, D. D. Chu, X. Liu, R. An, S. L. Pan and Z. H. Yang, Sulfate Derivatives with Heteroleptic Tetrahedra: New Deep-Ultraviolet Birefringent Materials in which Weak Interactions Modulate Functional Module Ordering, *Angew. Chem., Int. Ed.*, 2024, e202413680.

39 Z. Li, C. C. Jin, C. Y. Liu, J. J. Lu, Z. H. Yang, S. L. Pan and M. Mutailipu, $[B_3O_3F^4(OH)]^{2-}$: A Versatile Hydroxyfluorooxoborate Heteroanion Producing Compounds with Highly Tunable Optical Anisotropy, *Chem. Mater.*, 2024, **36**, 6985–6993.

40 C. H. Hu, M. F. Wu, M. Zhang, J. Han, X. L. Hou, F. Zhang, Z. H. Yang and S. L. Pan, "Cation Activation": An Effective Strategy for the Enhancement of Birefringence, *Adv. Opt. Mater.*, 2023, **11**, 2300579.

41 W. B. Zhang, M. Arif, H. Zhou, R. An, Z. H. Yang, X. L. Hou, S. L. Pan and S. J. Han, Highly Polarizable Phosphorus-Centered Tetrahedra and π-Conjugated Carbon-Centered Triangular Moieties Inducing Large Anisotropy and Short-Wavelength Phase-Matching, *Adv. Opt. Mater.*, 2025, **2403372**, 1–9.

42 C. H. Hu, H. M. Li, G. S. Xu, Z. H. Yang, J. Han and S. L. Pan, The New Paradigm of Ligand Substitution-Driven Enhancement of Anisotropy from SO_4 Units in Short-Wavelength Region, *ACS Cent. Sci.*, 2024, **10**, 2312–2320.

43 C. C. Jin, X. P. Shi, H. Zeng, S. J. Han, Z. Chen, Z. H. Yang, M. Mutailipu and S. L. Pan, Hydroxyfluorooxoborate Na

5342 | *Inorg. Chem. Front.*, 2025, **12**, 5335–5343

This journal is © the Partner Organisations 2025

$[B_3O_3F_2(OH)_2]\cdot[B(OH)_3]$: Optimizing the Optical Anisotropy with Heteroanionic Units for Deep Ultraviolet Birefringent Crystals, *Angew. Chem., Int. Ed.*, 2021, **60**, 20469–20475.

44 X. L. Chen, B. B. Zhang, F. F. Zhang, Y. Wang, M. Zhang, Z. H. Yang, K. R. Poeppelmeier and S. L. Pan, Designing an Excellent Deep-Ultraviolet Birefringent Material for Light Polarization, *J. Am. Chem. Soc.*, 2018, **140**, 16311–16319.

45 C. T. Chen, G. L. Wang, X. Y. Wang and Z. Y. Xu, Deep-UV nonlinear optical crystal $KBe_2BO_3F_2$—discovery, growth, optical properties and applications, *Appl. Phys. B*, 2009, **97**, 9–25.

46 G. Peng, N. Ye, Z. S. Lin, L. Kang, S. L. Pan, M. Zhang, C. S. Lin, X. F. Long, M. Luo, Y. Chen, Y. H. Tang, F. Xu and T. Yan, $NH_4Be_2BO_3F_2$ and $\gamma-Be_2BO_3$: Overcoming the Layering Habit in $KBe_2BO_3F_2$ for the Next–Generation Deep–Ultraviolet Nonlinear Optical Materials, *Angew. Chem., Int. Ed.*, 2018, **57**, 8968–8972.

47 G. Q. Shi, Y. Wang, F. F. Zhang, B. B. Zhang, Z. H. Yang, X. L. Hou, S. L. Pan and K. R. Poeppelmeier, Finding the Next Deep-Ultraviolet Nonlinear Optical Material: $NH_4B_4O_6F$, *J. Am. Chem. Soc.*, 2017, **139**, 10645–10648.

48 X. F. Wang, F. F. Zhang, L. Gao, Z. H. Yang and S. L. Pan, Nontoxic KBBF Family Member $Zn_2BO_3(OH)$: Balance between Beneficial Layered Structure and Layer Tendency, *Adv. Sci.*, 2019, **6**, 1901679.

49 Y. X. Song, M. Luo, D. H. Lin, C. S. Lin, Z. J. Wang, X. F. Long and N. Ye, π-Conjugated Trigonal Planar $[C(NH_2)_3]^+$ Cationic Group: A Superior Functional Unit for Ultraviolet Nonlinear Optical Materials, *ACS Omega*, 2021, **6**, 9263–9268.

50 X. Wen, Y. C. Yan, J. Y. Lu, X. M. Shi, P. Tang, J. D. Chen, G. S. Yang, G. Peng, H. H. Yu, H. J. Zhang, Z. G. Hu, J. Y. Wang and N. Ye, $[C_2N_4H_7O][NH_2SO_3]$: High–performance Ultraviolet Nonlinear Optical Crystal with Ditrigon Coupled Guanylurea Group, *Angew. Chem., Int. Ed.*, 2025, e202424153.

51 G. M. Sheldrick, A short history of SHELX, *Acta Crystallogr.*, 2008, **64**, 112–122.

52 A. L. Spek, Single-crystal structure validation with the program PLATON, *J. Appl. Crystallogr.*, 2003, **36**, 7–13.

53 S. J. Clark, M. D. Segall, C. J. Pickard, P. J. Hasnip, M. I. J. Probert, K. Refson and M. C. Payne, First principles methods using CASTEP, *Z. Kristallogr.*, 2005, **220**, 567–5770.

54 J. P. Perdew, K. Burke and M. Ernzerhof, Generalized Gradient Approximation Made Simple, *Phys. Rev. Lett.*, 1996, **77**, 3865.

55 H. J. Monkhorst and J. D. Pack, Special points for Brillouin-zone integrations, *Phys. Rev. B*, 1976, **13**, 5188–5192.

56 P. Kubelka and F. Munk, on Optics of Paint Layers, *Z. Tech. Phys.*, 1931, **12**, 593–601.

57 J. Tauc, Absorption edge and internal electric fields in amorphous semiconductors, *Mater. Res. Bull.*, 1970, **5**, 721–729.

58 H. Zhang, X. Jiang, Y. Zhang, K. Duanmu, C. Wu, Z. Lin, J. Xu, J. Yang, Z. Huang, M. G. Humphrey and C. Zhang, Toward Strong UV–Vis–NIR Second-Harmonic Generation by Dimensionality Engineering of Zinc Thiocyanates, *J. Am. Chem. Soc.*, 2024, **146**, 28329–28338.

59 Y. Liu, X. Liu, Z. Xiong, B. Liu, J. Xu, L. Li, S. Zhao, Z. Lin, M. Hong and J. Luo, 2D van der Waals Layered $[C(NH_2)_3]_2SO_3S$ Exhibits Desirable UV Nonlinear-Optical Trade-Off, *Inorg. Chem.*, 2021, **60**, 14544–14549.

60 Y. Li, W. Huang, Y. Zhou, X. Song, J. Zheng, H. Wang, Y. Song, M. Li, J. Luo and S. Zhao, A High–Performance Nonlinear Optical Crystal with a Building Block Containing Expanded π–Delocalization, *Angew. Chem., Int. Ed.*, 2023, **62**, e202215145.

61 Y. Li, X. Zhang, J. Zheng, Y. Zhou, W. Huang, Y. Song, H. Wang, X. Song, J. Luo, S. Zhao and S. Zhao, A Hydrogen Bonded Supramolecular Framework Birefringent Crystal, *Angew. Chem., Int. Ed.*, 2023, **62**, e202304498.

62 J. Cui, S. Wang, A. Tudi, M. Gai, Z. Yang and S. Pan, $(C(NH_2)_3)_2(I_2O_5F)(IO_3)(H_2O)$ and $C(NH_2)_3IO_2F_2$: Two Guanidine Fluorooxoiodates with Wide Band Gap and Large Birefringence, *Inorg. Chem.*, 2024, **63**, 661–667.

63 C. Chen, Y. Wu, A. Jiang, B. Wu, G. You, R. Li and S. Lin, New nonlinear-optical crystal: LiB_3O_5, *J. Opt. Soc. Am. B*, 1989, **6**, 616–621.

64 J. M. Tu and D. A. Keszler, $CsLiB_6O_{10}$: A noncentrosymmetric polyborate, *Mater. Res. Bull.*, 1995, **30**, 209–215.

This journal is © the Partner Organisations 2025

Inorg. Chem. Front., 2025, **12**, 5335–5343 | **5343**